

DESIGNED OPTIMUM GEOMETRY FOR MICRO-CHANNEL AND MICRO PIN FINS HEAT SINKS COOLING TECHNOLOGY

Bello-Ochende, T. and Meyer, J. P.

Department of Mechanical and Aeronautical Engineering
 University of Pretoria, Pretoria, Private Bag X20, Hatfield,
 0028, South Africa
 E-mail:tunde.bello-ochende@up.ac.za

ABSTRACT

This paper reports on the theoretical and geometric optimization of micro-channel heat sink and micro pin fins. Different types of micro-channel heat sinks and pin fins configuration were studied. In all the cases the objectives is to maximize the global thermal conductance subject to a fixed volume, high conducting material and a fixed pressure drop. In the first configuration the micro-channel is completely embedded inside a high conducting material and numerical simulations were carried out on a unit cell with volume ranging from 0.7 to 0.9 mm³ and pressure drop between 10 and 75 kPa. The axial length of the micro-channel heat sink was fixed at 10 mm. The cross-sectional area of the micro-channel heat sink is free to morph with respect to the degree of freedoms provided by the aspect ratio and the solid volume fraction. The effects of the total solid volume fraction and the pressure drop on the aspect ratio, channel hydraulic diameter and peak temperature are investigated. In the second configuration the micro-channels are embedded inside a high conducting material, except that the top is covered with an insulating material. The whole configuration was allowed to morph with respect to all the degrees of freedom. Similar but dimensionless numerical simulations were carried out on this configuration and the numerical optimization results were reported. In the first configuration numerical results show that the degrees of freedom have a strong effect on the peak temperature and the maximum thermal conductance. The optimal geometric characteristics (aspect ratio and the optimal channel shape) are reported and compared with those obtained from approximate relationships using scale analysis. For this configuration the predicted trends are found to be in good agreement with the predicted results. In the second configuration a test case on an actual micro-channel heat sink shows a reduction of about 8% in global thermal resistance.

In the third part of the report we use constructal theory to discover the geometry and spacing between two rows of pin fins rows so that the total heat transfer rate is maximized. The heat transfer across the fins is by laminar forced convection bathed by a free-stream that is uniform and

isothermal. The optimization is subjected to fixed total volume of fin materials. The dimensions of the optimized configuration are the result of balancing conduction along the fins with convection transversal to the fin. The resulting flow structure has multiple scales that are distributed non-uniformly through the flow structure. The results predicted based on scale analysis are in good agreement with the numerical results. The results also show that the flow structure performs best when the-fin diameters and heights are non-uniform.

Keywords: Constructal, Micro-channel heat sinks, Conductance, Optimal geometry, conjugate, fins, constructal, multiscale design, optimized configuration, heat transfer augmentation, extended surfaces, heat transfer density

Nomenclature

A	[m]	channel cross-sectional area
Be	[-]	Bejan number based on a unit volume, $\Delta PV^{2/3}/\alpha\mu$
Be_L	[-]	Bejan number based on L , $\Delta PL^2/\alpha\mu$
B	[m]	channels width
C	[-]	dimensionless global conductance
C_p	[J / kgK]	specific heat at constant pressure
D_1	[m]	diameter of the first fin
D_2	[m]	diameter of the second fin
D_3	[m]	diameter of the second fin
D_h	[m]	hydraulic diameter
f	[-]	friction factor
G	[m]	width of computational domain ($B + t_f$)
\bar{h}	[W/m ² k]	average heat transfer coefficient
H	[m]	height
H_1	[m]	height of the first fin
H_2	[m]	height of the second fin
H_3	[m]	height of the third fin

H_c	[m]	channel height
k	[W / mK]	thermal conductivity
L	[m]	axial length
n	[-]	normal
num	[-]	number of channels
P	[Pa]	pressure
P_c	[m]	perimeter of micro-channel
Po	[-]	Pousiele number
Pr	[-]	Prandtl number
q	[W]	total heat transfer
q''	[W / m ²]	heat flux
R	[K m/W]	thermal resistance
Re_{Dh}	[-]	Reynolds number based on hydraulic diameter
Re_L	[-]	Reynolds number based on L
S_1	[m]	spacing between the first cylinder and the trailing edge
S_2		spacing between the D_1 and D_2 cylinders
T	[⁰ C]	temperature
$T_{w,L}$	[⁰ C]	exit temperature
T_{in}	[⁰ C]	inlet temperature
T_{max}	[⁰ C]	maximum temperature
t_1	[m]	half thickness of vertical solid
t_2	[m]	base thickness
t_3	[m]	top thickness
U	[m/s]	average velocity
\vec{U}	[m/s]	velocity vector
U_∞	[m/s]	Free stream velocity
V	[m ³]	volume
W	[m]	heat sink width
x,y,z	[m]	Cartesian coordinates

Greek Symbols

α	[m ² / s]	thermal diffusivity
Δ	[-]	difference
μ	[kg.s / m]	viscosity
ν	[m ² / s]	kinematic viscosity
ρ	[kg / m ³]	density
ϕ	[-]	volume fraction of solid material (porosity)
τ	[Pa]	shear stress
Ω	[-]	interface between the solid and fluid

Subscripts

c	[-]	channel
f	[-]	fluid
h	[-]	hydraulic diameter
in , ∞	[-]	inlet
m	[-]	maximized once
3m	[-]	Maximixed thrice

max	[-]	maximum
min	[-]	minimum
opt	[-]	optimum
out	[-]	outlet
s	[-]	solid

Subscripts

~	[-]	dimensionless
---	-----	---------------

1. INTRODUCTION

The quest for better designs for the cooling of heat-generating devices has been a driving force for innovation and new fundamentals for heat transfer engineering and science. Micro-channels and micro pin fins are currently at the forefront of cooling technologies, because of the difficulties of meeting with air-cooling techniques the cooling needs of devices with high heat flux (projected to exceed 100 W/cm²) [1-3]. In modern heat transfer, the challenge is how to cool, manufacture, decrease cost and optimise performance. To solve these problems, several novel techniques have been proposed and studied theoretically, numerically and experimentally. A review of these techniques has been conducted by Dirker *et al* [1].

With the recent development of reliable numerical packages and their easy availability, optimisation of coupled convective flow (forced and natural) and conduction heat transfer has become easier to implement, and more popular. A review of the subject has been given by Bejan [4, 5], which focuses on the generation of shape and structure in freely morphing convective systems, by maximising global performance subject to global constraints. This view is known as constructal theory. An area where this theory is of the utmost importance is in heat transfer augmentation [6-9] where volumes reserved for fluids that act as a heating or cooling agent are optimised.

Significant research [10-36] has also been conducted on the flow and heat transfer characteristics of micro-channel heat sinks and micro pin fins, because of their promise to cool areas with high heat flux. These studies relied on numerical techniques and experiments [11-19, 27-36] to study the flow and heat transfer characteristics of micro-channel heat sinks.

In the present paper, starting from a basic construction unit (the elemental volume is the constructal approach); we determined numerically the best possible geometry for two types of micro-channel heat sink configurations and micro pin fins heat sink. The total elemental volume and axial length of the micro-channel heat sink were fixed. For the pin fin heat sink, the total volume and pin fins materials was fixed. We sought to determine the best channel dimensions and system configurations that minimise the peak temperature when the pressure difference across the elemental volume is fixed.

MICRO-CHANNEL EMBEDDED INSIDE A HIGH CONDUCTING SOLID

Figure 1a shows a drawing of the physical model and the computational domain for a micro-channel heat sink. Heat is supplied to a highly conductive silicon substrate with known thermal conductivity from a heating area located at the bottom of the heat sink. The heat is then removed by a fluid flowing through a number of micro-channels. Using the advantage of symmetry, we selected for analysis an elemental volume (unit cell) consisting of a micro-channel and the surrounding solid, as is shown in Fig. 1b. This work was based on the model of Qu and Mudawar [12] and Kawano *et al* [17].

The heat transfer in the elemental volume is a conjugate problem that combines heat conduction in the solid and convective heat transfer in the liquid. The two heat transfer mechanisms are coupled through the continuity of temperature and heat flux at the interface between the fluid and the solid. The fluid with inlet temperature, T_{in} is driven through the micro-channel by a fixed pressure difference $\Delta P = P(z = 0) - P(z = L)$, which is maintained between the channel inlet and outlet. The objective of the following analysis was to determine the heat transfer characteristics for a given micro-channel, and the best possible configuration ($L, t_1/t_2, t_2/t_3, H/G$) that corresponds to the maximal global thermal conductance, or global minimal thermal resistance.

The following assumptions were made to model the heat transfer and fluid flow in the elemental volume: the hydraulic diameter of the micro-channel under analysis is greater than $10 \mu\text{m}$; for water, the continuum regime applies hence the Navier-Stokes and Fourier equations can still be used to describe the transport processes; steady-state conditions for flow and heat transfer; incompressible flow; the properties of the solid and fluid are constant; and the heat transfer due to radiation and natural convection is negligible. It is also assumed that the number of elemental micro-channels is large. Based on these assumptions, the continuity, momentum and energy equations for the cooling fluid are

$$\nabla(\rho\vec{U}) = 0 \quad (1)$$

$$\rho(\vec{U} \cdot \nabla\vec{U}) = -\nabla P + \mu\nabla^2\vec{U} \quad (2)$$

$$\rho C_p(\vec{U} \cdot \nabla T) = k_f \nabla^2 T \quad (3)$$

where $\nabla^2 = \partial/\partial x^2 + \partial/\partial y^2 + \partial/\partial z^2$, and the origin of the Cartesian frame (x, y, z) is located in the bottom left-hand corner of the computational domain, where \vec{U} is the velocity vector, T is temperature, P is pressure, μ is the viscosity, k_f is the thermal conductivity of the fluid and ρ is the density of the fluid. For the volume occupied by a solid, the momentum equation is simply

$$\vec{U} = 0 \quad (4)$$

and the energy equation is

$$k_s \nabla^2 T = 0 \quad (5)$$

Where k_s is the thermal conductivity of the solids.

The entire elemental volume is treated as a continuous domain. The geometric boundary conditions for the computational domains are indicated in Fig. 1b. The flow boundary conditions are such that no-slip occurs on the walls inside the channel. At the entrance of the channel, the pressure boundary conditions become

$$P = \frac{\alpha\mu Be}{V^{2/3}} + P_{out} \quad (6)$$

where Be is the dimensionless pressure drop number based on the elemental volume (the Bejan number, cf. Refs. [20, 21]). $P = 1 \text{ atm}$, at the channel outlet, and $T = 20 \text{ }^\circ\text{C}$ at the channel inlet, V is the volume of the elemental unit. The thermal boundary conditions consist of an assumed uniform heat flux (q'') that is imposed at the bottom of the heat sink

$$k_s \frac{\partial T}{\partial y} = -q'' \quad (7)$$

The remaining outside walls and the plane of symmetry of the heat sink were modelled as adiabatic. The continuity of the temperature and flux at the interface of the solid and fluid surfaces requires

$$-k_s \frac{\partial T_s}{\partial n} \Big|_{\Omega} = -k_f \frac{\partial T}{\partial n} \Big|_{\Omega} \quad (8)$$

Where, in each case, n is the direction normal to the wall and Ω is the interface fraction of the solid and fluids. The shapes of the heat sink and cooling channels were allowed to vary, by changing G, H, t_1, t_2 and t_3 .

We maximises the overall global thermal conductance of the geometry, which in dimensionless form is defined as

$$C = \frac{q''L}{k(T_{max} - T_{in})} \cong \frac{q''L}{k(T_{w,L} - T_{in})} \quad (9)$$

Here q'' is the heat flux from the base of the micro-channel heat sink, k is the thermal conductivity of the fluid, and L is the length of the computational domain of the unit volume. The global conductance C is a dimensionless way of expressing the ratio of the total heat transfer rate q divided by the largest excess temperature ($T_{w,L} - T_0$) reached at any point in the micro-channel heat sink. The maximum temperature is expected to occur in the exit plane of the micro-channel heat sink. The reciprocal of C is the dimensionless global thermal resistance.

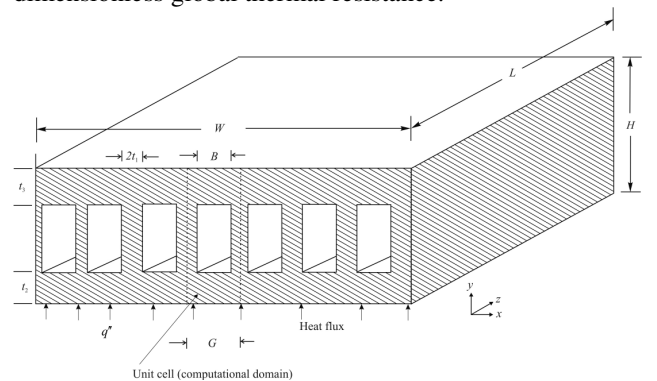


Figure 1a

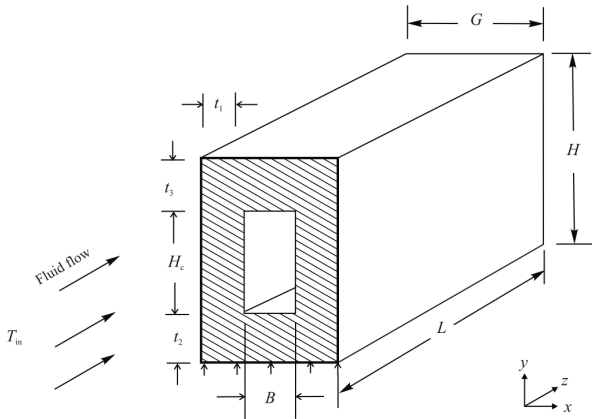


Figure 1b Micro-channel computational unit cell of a heat sink and the computational domain of a micro-channel heat sink.

Table 1 Dimensions of micro-channel heat sink Ref. (12)

Case	H/ μm	t ₁ / μm	t ₂ / μm	ϕ
1	900	22.5	270	0.6638
	H-(t ₂ +t ₃)/ μm	(G-2t ₁)/ μm	G/ μm	L/mm
	900	22.5	100	10mm

Numerical Method and Code Validation

The finite volume method was used to solve the continuity, momentum and energy equations. A detailed explanation is given in Patankar [22]. In the finite volume method, the domain is divided into a number of control volumes such that there is one control volume surrounding each grid point. The grid point is located in the centre of the control volume. The governing equation is integrated over each control volume to derive algebraic equations containing a point value of the dependent variable at the grid point. The discretised equations express the conservation principle for a finite volume.

The second order upwind scheme was used to model the combined convection-diffusion effect in the transport equations. The resulting algebraic equations were solved using a line-by-line tri-diagonal matrix inversion algorithm. The SIMPLE algorithm [22] was then applied to solve the coupled systems of equations.

Convergence is obtained when the residuals for the mass and momentum equation are smaller than 10^{-4} , and the residual of the energy equation becomes less than 10^{-9} . A grid-independence test was carried out for the micro-channel heat sink with the dimension given in Table 1. Tests show that a control volume with a mesh size of 25 in the x -direction, 50 in the y -direction and 150 in the z -direction assures a grid independent solution in which the maximum thermal resistance changes less than 2.5% when the mesh is sequentially doubled. This mesh also guaranteed that the numerical results obtained in this work are comparable with predictions and data obtained from experimental and numerical work.

The numerical results generated were compared with the numerical results of Qu and Mudawar [12] for their case when the heating component in Fig. 1 was placed on top of the micro-channel heat sink. Figure 2 compares the thermal resistances, R , for both the inlet and the outlet resistance. The comparison was made using the Reynolds number

based on the hydraulic diameter in the range $90 \leq Re_{Dh} \leq 400$. These parameter are defined as

$$R(x) = \frac{T(x) - T_0}{q''} \quad (10)$$

where x is distance from the entrance, which in this case are located at $x = 0$, and $x = L$. The Reynolds number

$$Re = \frac{UD_h}{\nu} \quad (11)$$

From eqn (11), ν is the kinematic viscosity, and the hydraulic diameter are

$$D_h \equiv \frac{4A_c}{P_c} = \frac{4BH_c}{2(B+H_c)} = \frac{4(H-(t_2+t_3)) \times (G-2t_1)}{2(H+G-(2t_1+t_2+t_3))} \quad (12)$$

where A_c is the channel cross-sectional area and P_c is the perimeter of the micro-channel. Figure 2 shows that the present numerical model captures the work of Qu and Mudawar¹², and it predicts very well the inlet and outlet thermal resistances. The maximum difference is 1.8% for the inlet and 1.5% for the outlet. Note also that Qu and Mudawar [12] validated their result by comparing it with the experimental data of Kawano *et al* [17].

Once the model adopted in this work had been validated, numerical optimisation was conducted to determine the optimal geometry of the micro-channel using the constrained optimisation outlined in the next section. The above code verification and grid-independence test provide confidence in the numerical code used in this work.

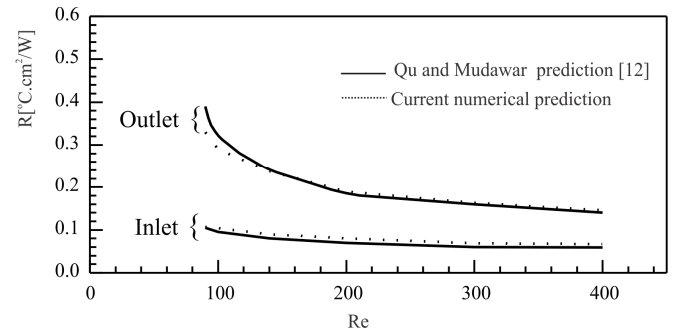


Figure 2 Comparison of numerical predictions at inlet thermal resistance, and outlet thermal resistance.

Optimisation Constraints and Parameters

In the present research, we applied constructal theory to an arbitrary unit of a micro-channel heat sink with a fixed given volume (length and cross-sectional area), and substrate material. The only parameter that was allowed to vary is the cross-sectional shape of the micro-channel heat sink, and the ratio of the internal thickness of the vertical and horizontal substrate.

The elemental volume constraint for a given computational cell is

$$GHL = V \text{ (constant)} \quad (13)$$

and the volume of the solid substrate is

$$2Ht_1L + (G - 2t_1)Lt_2 + (G - 2t_1)t_3L = V_s \quad (\text{constant}) \quad (14)$$

For a fixed length we have,

$$GH = \frac{V}{L} = A \quad (\text{constant}) \quad (15)$$

The volume of the micro-channel is therefore

$$V_f = V - V_s \quad (\text{constant}) \quad (16)$$

Equation (15) can also be expressed in terms of the solid volume fraction, $\phi = V_s/V = A_s/A$. Equations (14) - (16) were solved simultaneously for t_1 , t_2 and t_3 , such that for any changes in the assumed thickness and geometric parameters, the aspect ratios (t_1/t_2 , t_2/t_3 , H/G and ϕ), the total volume, and volume of solid substrate remain fixed. The volume remains fixed, the cross-sectional shapes of the micro-channel heat sink change in such a way that the solid substrate conducts the heat from the base such that the thermal resistance is minimised. The total number of micro-channels in the micro-channel heat sink arrangement is obtained from

$$num = \frac{W}{B + 2t_1} \quad (17)$$

for a fixed total width, W .

Scale analysis and the intersection of asymptotic method

In this section, we present the use of a scaling argument to predict the optimal channel geometry that minimises the global thermal resistance or the maximum global thermal conductance. The following assumptions were made throughout the analysis: uniform flow distribution (equal flow in all the channels, constant cross-sectional area of the channels, and no inlet or exit plenum losses), the Prandtl number range $Pr > 0.5$, negligible axial conduction, and the thermal conductivity of the solid substrate being much greater than that of the fluid. The existence of an optimal arrangement can be expected based on the trade-off demonstrated in the forced convection cooling of electronics packages [8], and the method outlined by Muzychka[23]. To determine the optimal channel dimensions, we used the method of intersection of asymptotes [7] for a unit micro-channel as shown in Fig. 2. The global thermal conductance scales were evaluated in two extreme limits (small channel and large channel).

The method of intersection of the asymptotes outlined by [23-26] was used for determining the optimal duct shape. In the limit of small channels the expression for dimensionless global thermal conductance is

$$C_{\text{small}} = 0.25 \frac{D_h^2}{LV^{1/3}} \frac{Be}{Po} \quad (18)$$

The above expression shows that for small channels, the dimensionless thermal conductance, C_{small} , is directly proportional to D_h^2 [26].

In the opposite extreme, for large channels, the flow is essentially a boundary-layer flow, and the global thermal conductance becomes

$$C_{\text{large}} = 1.31 \frac{V^{1/9} L^{1/3}}{D_h^{2/3}} Be^{1/3} \quad (19)$$

The above expression shows that, C_{large} is directly proportional to $D_h^{-2/3}$. The optimal channel shape can be

approximated as the D_h value where the two equation curves intersect,

$$D_{h,opt} \approx 1.86 \left(L^3 V \right)^{1/6} Po^{3/8} Be^{-1/4} \quad (20)$$

Po can be approximated using a single-term approximation for the Poiseuille number [23-26] for $H_c > B$

$$Po = \frac{12}{\left(1 + \frac{B}{H_c} \right)^2 \left[1 - \frac{192}{\pi^5} \frac{B}{H_c} \tanh\left(\frac{\pi H_c}{2B} \right) \right]} \quad (21)$$

Equation (20) can be introduced in equation (18) or equation (19) to determine the maximum dimensionless global thermal conductance

$$C_{\text{max,theoretical}} \approx 0.864 \frac{Be^{1/2}}{Po^{1/4}} \quad (22)$$

As shown above, the intersection of asymptotes method and scale analysis are powerful tools that allow engineers and scientists to estimate trends and optimal configurations [see Ref. [7]]. It is important, though, to understand the limits of the theoretical results obtained from equations (20 and 22). They are only rough estimates of the results and trends. They have to be compared with the results obtained from numerical optimisation. Furthermore, the above relations are valid for large Be and according to Knight *et al.*[13], the realistic dimensionless pressure drop number through micro-chips should be typically in the range of 10^8 and 10^{12} .

Results: Numerical result for optimal geometry for micro-channel heat sinks

In the preceding section, an approximate method was used to determine the optimal channel shape that minimises the global thermal conductance. A series of numerical optimisations and calculations was conducted in this section, and the results are presented in order to show the effects of pressure drop, solid materials and the effect of the external aspect ratio for a fixed set of internal aspect ratios (the ratio of base solid thickness to vertical thickness) on the optimal micro-channel geometry. Some important fluid flow and heat transfer parameters that were employed in this study are summarised in Table 1. The thermophysical properties of water used in this study were based on water at 20 °C. The volume of the micro-channel was fixed and it was based on the data given by Qu and Mudawar [12]. The thermal conductivity of the solid substrate (silicon) was taken to be 148 W/m K. The applied heat flux at the bottom of the micro-channel was fixed at 100 W/cm². We sought to determine the best geometry that minimises the maximum excess temperature, T_{max} , or the overall global conductance.

The micro-channel heat sink has five degrees of freedom, L , H/G , t_1/t_2 , t_2/t_3 and ϕ . For this study, three degrees of freedom were fixed L , t_1/t_2 and t_2/t_3 , while the other two were allowed to vary with the assumed pressure drop. In the first stage of the optimisation, we fixed the internal structure of the micro-channel by setting ($t_1/t_2 = 0.08$, $t_2/t_3 = 1$ and $\phi = 0.8$). The total volume of the unit micro-channel was set in the range $0.01 \text{ mm}^3 \leq V \leq 0.9 \text{ mm}^3$, the axial length of the micro-channel was fixed at 10 mm, and a unit cross-sectional area varied from 0.01 to 0.09 mm². The micro-channel heat sink was expected to occupy a total base surface area of 10 mm × 10 mm.

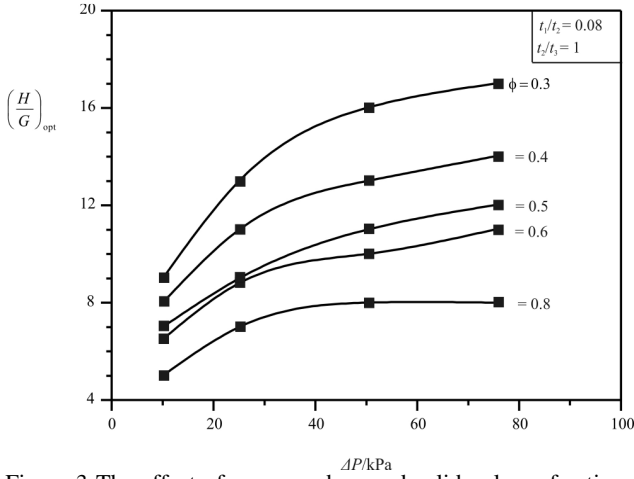


Figure 3 The effect of pressure drop and solid volume fraction on the optimised aspect ratio.

The pressure drop across a unit cell was set at 50 kPa, the total unit volume of 0.9 mm^3 was used for the first optimisation. The aspect ratio (H/G) was optimised for a fixed ϕ . This procedure was repeated for different values of ϕ . Figure 3 summarises the effect of pressure drop on the optimal external aspect ratio, in the range $10 \text{ kPa} \leq \Delta P \leq 75 \text{ kPa}$. For a fixed solid fraction, the optimal external aspect ratio exhibits two types of behaviour, as shown in Fig. 3. At low pressure drops, the optimised $\left(\frac{H}{G}\right)_{\text{opt}}$ increases with an increase in the pressure drop, while for $\Delta P \geq 50 \text{ kPa}$, $\left(\frac{H}{G}\right)_{\text{opt}}$ increases slightly with increases in the pressure drop, and is almost invariant for $\phi = 0.8$. Similarly, the optimised external aspect ratio $\left(\frac{H}{G}\right)_{\text{opt}}$ decreases with an

increase in the solid volume fraction for the range of geometric parameters used in this study. As the aspect ratio increases, the cross-sectional area of the micro-channel becomes slender in the vertical direction and the value of the hydraulic diameter changes.

Figure 4 shows the behaviour of the optimal micro-channel geometry represented by the optimal hydraulic diameter. $D_{h,\text{opt}}$ decreases with an increase in the pressure drop, as suggested from the theoretical derivation of equation (20) for a fixed solid volume fraction, and decreases as the volume fraction increases. The minimum optimal hydraulic diameter is more than $100 \mu\text{m}$. For the entire range, the optimal hydraulic diameter lies in the continuum region and gives us confidence in our continuum assumption.

Figure 5 describes the behaviour of the minimised maximum temperature difference ΔT_{min} with respect to the applied pressure drop. Note that ΔT_{min} decreases monotonically with increases in pressure drop. From Fig. 7, follows that an optimal arrangement of volume of solid fraction exists and lies in the vicinity of $\phi = 0.5$ and 0.4 .

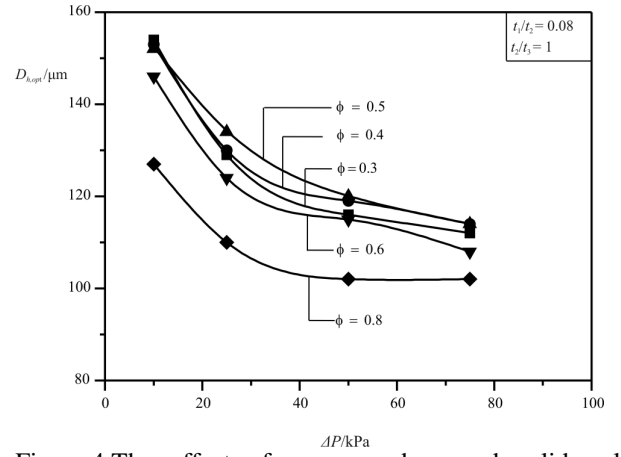


Figure 4 The effect of pressure drop and solid volume fraction on the optimised channel hydraulic diameter

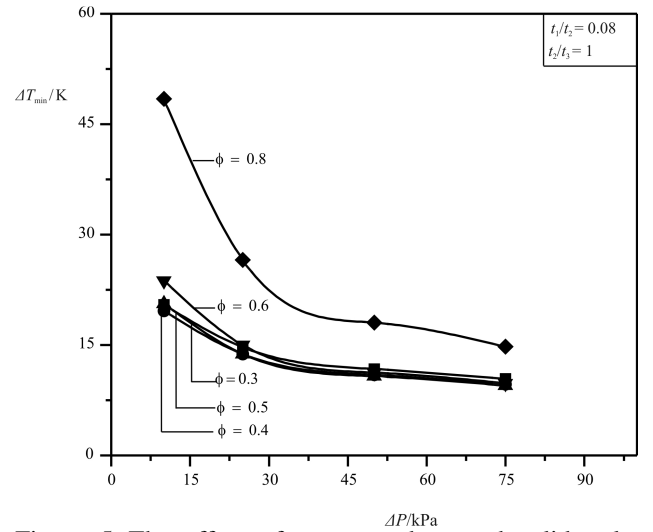


Figure 5 The effect of pressure drop and solid volume fraction on the minimised peak temperature difference.

For comparison, the scale prediction for the maximum heat transfer rate equation (22) is plotted against the global thermal conductance. The results are reported based on the dimensionless global conductance equation (9) and dimensionless pressure drop number, Be , equation (6). The maximised global thermal conductance increases with an increase in Be .

Figure 6 shows the comparison between the theoretical solution equation (22) and the numerical solution. The numerical results follow the trend predicted by equation (22), but over-predict the numerical value by a factor of 8, this is due to the simplifying assumptions used in deriving the theoretical solution. For $\phi = 0.5$, the numerical maximised global thermal conductance can be correlated within 0.05% with the power law

$$C_{\text{max}} = 0.82Be^{0.38} \quad (23)$$

While for equation (22) and Fig. 6, the results are represented by the power law

$$C_{\text{max, theory}} = 0.6Be^{0.49} \quad (24)$$

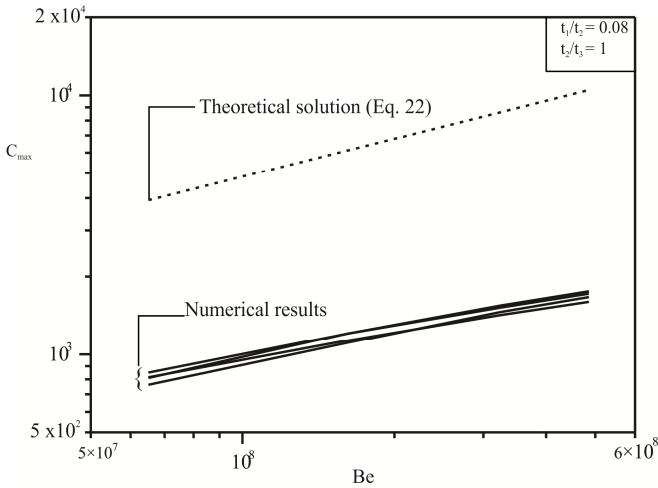


Figure 6. The effect of dimensionless pressure drop number and solid volume fraction on the dimensionless global thermal conductance

Figure 7 shows a comparison between the optimal duct shape, $D_{h,opt}$ obtained numerically and the analytical prediction equation (20). The trend is the same for both solutions. The theoretical and numerical values agree within 1% for the best case, and within less than 10 % for the worst case. These results are in agreement with previous work on the construal method [5, 9, 23-26], according to which maximum heat transfer density means optimal packings in which the flow regions that do not contribute to global performance are eliminated.

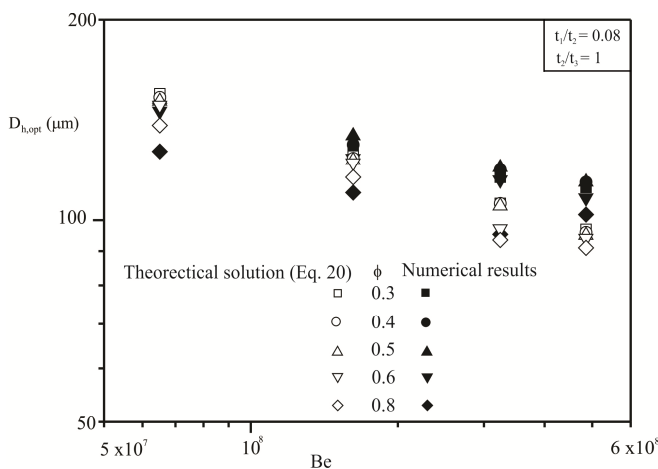


Figure 7 The optimal micro-channel shape (hydraulic diameter) for maximum global conductance.

CASE STUDY 1: Application to Micro-channel with variable Length

When the axial length that was fixed previously at 10mm was relaxed, [c.f. Refs [34, 36] and a mathematical optimisation program were then used to determine the optimal micro-channel geometry. Table 2 shows the results of the optimized geometry as a function of the applied pressure drop. The behaviour of the optimized channel aspect ratio, the hydraulic diameter, the ratio solid volume to total volume are reported in Table 2a, also showing in Table 2b are the optimized geometry when the volume of the unit cell was varied between 0.7 and 0.9 mm³. The optimal configuration provides improved heat transfer

capability with an increased in maximized global thermal conductance of the heat sink of up to 20% at low pressures. Figure 8 show that the increased in the degree of freedom as a results of relaxing the axial length. It prove to offer better optimal cooling effect at lower pressure drops with more than 16% decrease in optimal peak temperature.

Table 2a. Optimal design results when the axial length is relaxed

Pressure Drop (kpa)	$(H_c/B)_{opt}$	ϕ_{opt}	$(D_h)_{opt}$	C_{max}
60	11.831	0.440	0.126	1884.33
50	11.341	0.439	0.131	1790.59
40	10.753	0.439	0.139	1683.47
30	10.079	0.429	0.149	1543.51
20	9.170	0.407	0.161	1354.90
10	7.873	0.382	0.188	1081.83

Table 2b. Optimal design results for various computational volumes

Volume (mm ³)	Minimized Temp. (°C)	$(H_c/B)_{opt}$	ϕ_{opt}	$(D_h)_{opt}$ (mm)
0.9	29.53	11.752	0.425	0.122
0.8	29.79	10.069	0.425	0.123
0.7	30.12	10.359	0.386	0.118

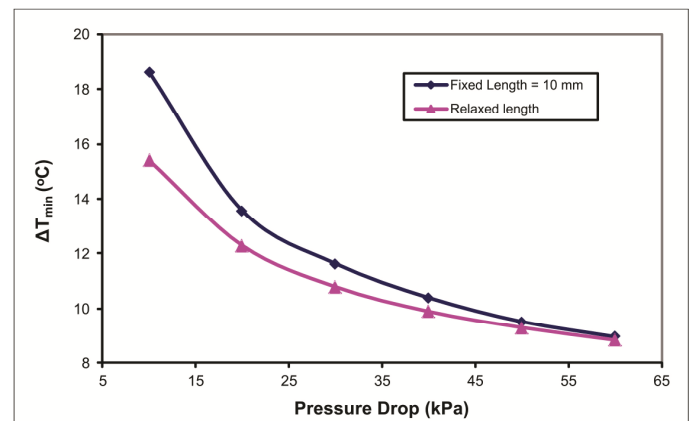


Figure 8 The effect of the relaxation of the axial length as compared to the fixed length optimal peak wall temperature difference

MICRO-CHANNEL EMBEDDED INSIDE A HIGH CONDUCTING MATERIAL AT THE SIDES AND INSULATION COVER ON THE TOP

Figure 9 shows a schematic drawing of the physical model and the computational domain for a heat sink cooling channel capped with a cover plate that is a relatively poor thermal conductor. Heat was supplied to the high conductivity substrate (solid) from a heating area located at the bottom of the heat sink. It was then removed by a fluid flowing through a number of cooling channels, as shown in Figure 9. Using the advantage of symmetry, we selected for analysis a unit cell consisting of a channel and the surrounding solids, as is shown in Fig. 10. Attention was focused on the heat transfer optimisation of this unit cell, and the results were extended to the remaining cooling channels.

The heat transfer in the unit cell is a conjugate problem that combines heat conduction in the solid and convective heat transfer in the fluid. The two heat transfer mechanisms were coupled through the continuity of temperature and flux at the interface between the fluid and the solid. The fluid was driven through the channel by a fixed pressure difference $\Delta P = P(z=0) - P(z=L)$, which was maintained between the channel inlet and outlet. This is a good model for electronic systems in which several packages and the channels receive their coolant in parallel from the same plenum. The channel was bathed by a single-phase stream of inlet temperature T_0 . The objective of the following analysis was to determine the optimal geometry ($L, t_1/t_2, H/G$, where $G = B/2 + t_1$), which correspond to the maximal global thermal conductance. As in other constructal studies, Bejan [4, 30, 32] and Bejan and Almgel [30], in the present work the search for configuration was subjected to two global constraints:

the elemental total volume constraint for a unit cell,

$$GHL = V \text{ (constant)} \quad (25)$$

and the volume of the solid substrate,

$$(H - t_2)Lt_1 + GLt_2 = V_s \text{ (constant)} \quad (26)$$

The volume of the fluid channel is

$$V_f = V - V_s \text{ (constant)} \quad (27)$$

were the solid volume fraction, $\phi = V_s/V$.

The following assumptions were made; the number of cooling channels was large; the model chosen for analysis was located at the centre of the heat sink and cooling channel arrangement, hence heat spreading is minimized [11, 26-32].

Equations (1) to (8) and (25) to (27) are non-dimensionalized by using $V^{1/3}$ as the length scale and, $q''V^{1/3}/k$ as the temperature scale. The non-dimensionalization of the governing equations is achieved by defining the variables

$$(\tilde{x}, \tilde{y}, \tilde{z}, \tilde{L}, \tilde{H}, \tilde{G}, \tilde{t}_1, \tilde{t}_2) = \frac{(x, y, z, L, H, G, t_1, t_2)}{V^{1/3}} \quad (28)$$

$$(\tilde{u}, \tilde{v}, \tilde{w}) = \frac{(u, v, w)}{\Delta P V^{1/3} / \mu} \quad (29)$$

$$\tilde{T} = \frac{T - T_0}{q''V^{1/3}/k}, \quad \tilde{P} = \frac{P}{\Delta P} \quad (30)$$

The total volume and solid volume constraints reduce to

$$\begin{aligned} \tilde{G}\tilde{H}\tilde{L} &= 1 \\ (\tilde{H} - \tilde{t}_2)\tilde{L}\tilde{t}_1 + \tilde{G}\tilde{L}\tilde{t}_2 &= \phi \end{aligned} \quad (31)$$

The entire unit cell was treated as a unitary (continuous) domain. The boundary conditions for the computational domains are indicated in Figure 10, where the plastic cover was assumed to have zero thickness. The flow boundary conditions are: no-slip on the walls inside the channel; $\tilde{P} = 1$ at the entrance of the channel, $\tilde{P} = 0$ at the channel outlet,

and $\tilde{T} = 0$ at the channel inlet. The thermal boundary conditions consist of a uniform heat flux, $\tilde{q} = 1$, which is imposed at the bottom of the heat sink

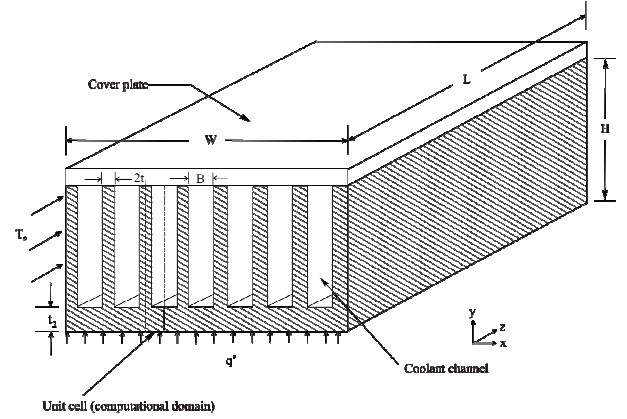


Figure 9 Heat sinks with rectangular cooling channel and the computational unit cell.

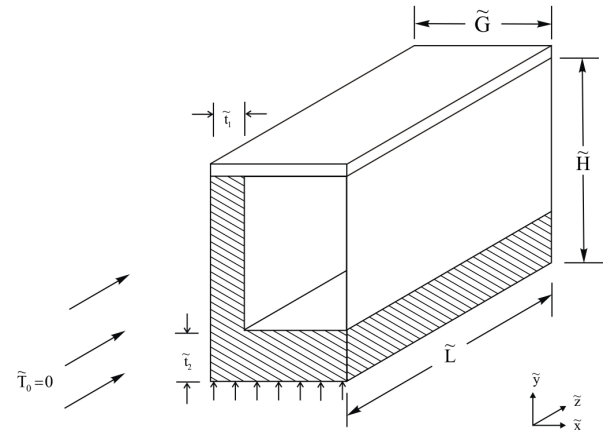


Figure 10 Computational domain of heat sink and a cooling channel with fixed volume and variable shape.

$$\tilde{q} = \frac{k(\partial T / \partial n)_{n=0}}{q''} \quad (32)$$

where n is the normal to the walls. The remaining outside walls and the plane of symmetry of the heat sink were modelled as adiabatic. The continuity of the temperature and flux at the interface of the solid and fluid surfaces requires

$$-k_s \frac{\partial \tilde{T}_s}{\partial n} \Big|_{\Omega} = -k \frac{\partial \tilde{T}}{\partial n} \Big|_{\Omega} \quad (33)$$

where \tilde{k} is the conductivity ratio k_s/k .

The shape of the heat sink and cooling channels was allowed to vary, by changing \tilde{G} , \tilde{H} , \tilde{L} , \tilde{t}_1 and \tilde{t}_2 . Just as in the previous section, we were interested in the geometric arrangement that maximises the overall global thermal conductance of the geometry, which in dimensionless form is defined as

$$C = \frac{q''L}{k(T_{\max} - T_0)} = \frac{\tilde{L}}{\tilde{T}_{\max}} \quad (34)$$

The dimensionless global conductance measures the quantity of heat flow from the conjugate system per unit temperature between coolant inlet temperature and the peak temperature.

Optimal Geometry

Using the same numerical procedures described earlier, the micro-channel heat sink structure had three degrees of freedom, \tilde{L} , H/G , and t_1/t_2 . The values of Be , Pr , \tilde{k} and ϕ were kept fixed. The search for optimal flow and heat sink configurations was conducted in three nested optimisation loops. First, in the inner loop, we fixed \tilde{L} and H/G and optimised t_1/t_2 such that C reaches a maximum, C_{3m} . Figure 11 summarises the final stage of the optimisation procedure in the range $10^4 \leq Be \leq 10^6$. This figure shows that the maximum thermal conductance, C_{3m} and the optimal length, \tilde{L}_{opt} increase with Be . The optimal cross-sectional shape and the shape of the solid component are practically independent of Be , namely $\left(\frac{H}{G}\right)_{opt} \cong 7.5$

and $\left(\frac{t_1}{t_2}\right)_{opt} \cong 0.75$. From these results, we found that the cross-sectional shape of the cooling channel is also constant, $(H - t_2)/(G - t_1)_{opt} \cong 8.81$.

From Figure 11, we concluded that \tilde{L}_{opt} and C_{3m} vary as

$$\tilde{L}_{opt} \cong 0.24Be^{1/4} \quad (35)$$

$$C_{3m} \cong 0.91Be^{0.35} \quad (36)$$

In view of $\left(\frac{H}{G}\right)_{opt} \cong 7.5$ and the volume constraint given in

equation (31), the optimised length shown in equation (35) is equivalent to an optimal slenderness of the longitudinal profile

$$\left(\frac{L}{H}\right)_{opt} \cong 0.043Be^{3/8} \quad (37)$$

Eliminating V between equations (35, 37), the slenderness of the enclosure becomes

$$\left(\frac{L}{H}\right)_{opt} \cong 0.088Be_L^{1/4} \quad (38)$$

where the number Be_L is based on L , Bejan and Sciubba [9].

$$Be_L = \frac{\Delta PL^2}{\alpha\mu} \quad (39)$$

Note that equations (37 and 38) have the same form as the relationship obtained for the optimal slenderness of a thin heat-generating strip of width D bathed by a single-phase stream of cold fluid in a duct of fixed volume and longitudinal pressure drop, Bello-Ochende and Bejan [8]. Note further that equation (38) has a form similar to those obtained for the optimal spacing in stacks of parallel plates with convective heat transfer and fixed volume and pressure drop [30, 33]. Equation (38) proves the importance of Be as the dimensionless parameter in forced convection cooling problems with prescribed longitudinal pressure drop.

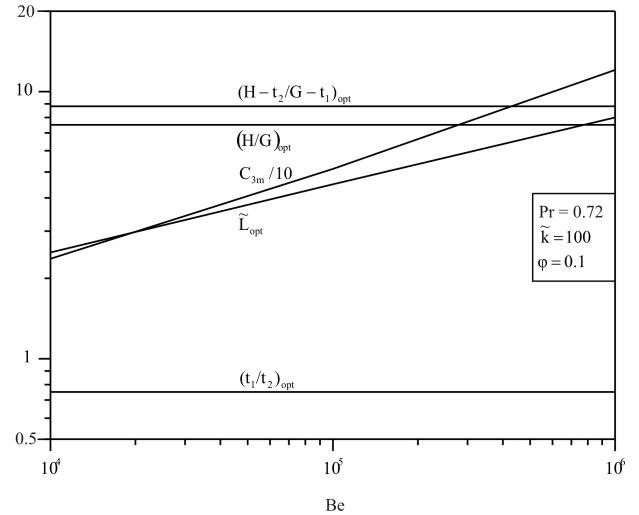


Figure 11 The effect of pressure drop number on the optimised heat sinks and coolant channel.

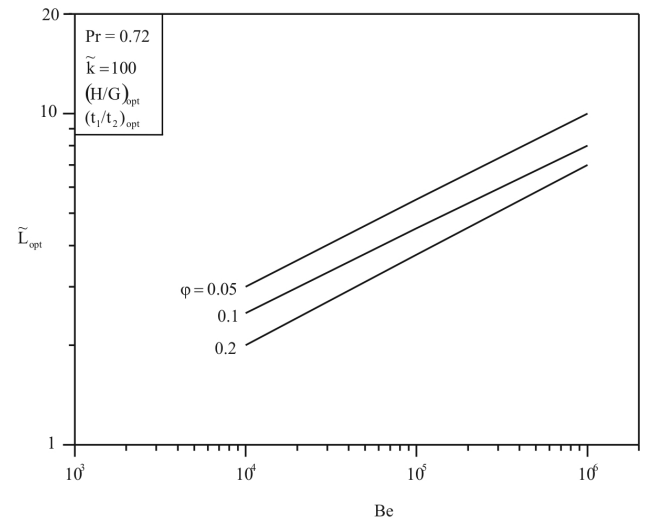


Figure 12 The effect of volume solid fraction and pressure drop number on the optimised longitudinal length.

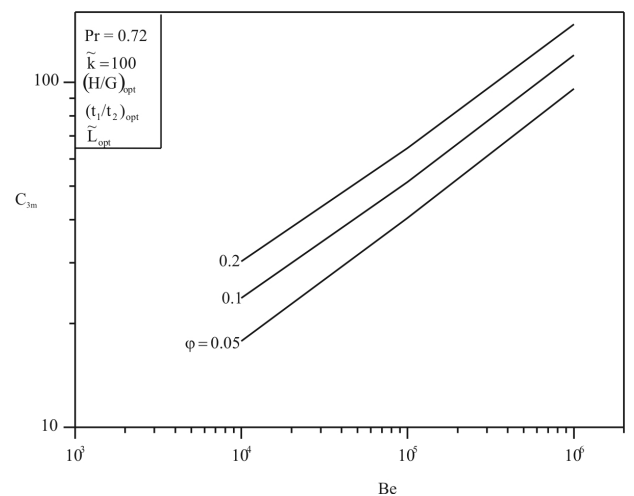


Figure 13 The effect of volume solid fraction and dimensionless drop number on the global thermal conductance.

Figure 12 shows the effects of the solid volume fraction ϕ on the optimised longitudinal lengths. It shows

that optimised longitudinal length increases with a decrease in ϕ , and increases as Be increases. In the range $0.05 \leq \phi \leq 0.2$ and $10^4 \leq Be \leq 10^6$, \tilde{L}_{opt} can be correlated with a standard deviation of 0.00334 by the expression,

$$\tilde{L}_{opt} \cong 0.144 \left(\frac{Be}{\phi} \right)^{0.25} \quad (40)$$

This correlation has the same form as the theoretical formula obtained by Ordonez [35]. Figure 13 shows the corresponding result for the maximised global conductance. The maximised global conductance increases as the solid fraction increases; this was expected as the available area used for conduction increases.

Next, we considered the important question of the effect of dimensionless thermal conductivity on an optimised structure and its corresponding global thermal conductance. The effect of thermal conductivity on the optimised structure is very interesting: Fig. 14 summarises the effect of \tilde{k} on the maximised global thermal conductance and the optimised structure for a fixed dimensionless pressure drop number, solid volume fraction and Prandtl number.

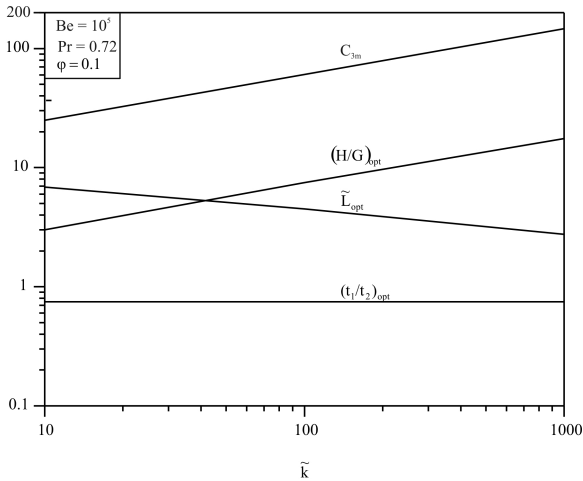


Figure 14 The effect of dimensionless thermal conductivity on the optimised parameters and global thermal conductance.

The figure shows that the internal ratio of the conducting solids (heat sink) does not vary much with \tilde{k} and it is approximately $(\tilde{t}_1/\tilde{t}_2)_{opt} = 0.75$. The optimum aspect ratio

$(H/G)_{opt}$ increases dramatically with an increase in \tilde{k} . This means that the optimised cross-section becomes longer while the optimised longitudinal length \tilde{L}_{opt} becomes shorter. When designing a heat sink cooling channel, the optimised external shape varies for different materials. This is because different materials have different conductivities and the design is not robust relative to the thermal conductivity and varies for different conductivities. As expected, the thrice-maximized global conductance, C_{3m} increases as \tilde{k} increases. The different effects of dimensionless thermal conductivity and dimensionless pressure drop on the optimised structure for a fixed Pr and ϕ are worth noting. A future challenge is to determine the conjugate system's competitiveness in terms of cost: the cost

of pumping the fluid through the cooling channels (pressure drop) and that of using conducting solid with high dimensionless thermal conductivities. The question is which is more profitable, increasing the pumping power or using materials with higher thermal conductivity for a fixed volume, as both increase the global thermal conductance but have different effects on the optimised structure.

Table 3 Dimensions of micro-channel heat sink Ref. (10, 11)

Case 1	H/ μm	$t_1/\mu\text{m}$	$t_2/\mu\text{m}$	ϕ
	533	22	213	0.6638
	H- $t_2/\mu\text{m}$	(G- $t_1)/\mu\text{m}$	G/ μm	L/mm
	320	28	50	10mm

Case 2	H/ μm	$t_1/\mu\text{m}$	$t_2/\mu\text{m}$	ϕ
	430	22.5	143	0.633
	H- $t_2/\mu\text{m}$	(G- $t_1)/\mu\text{m}$	G/ μm	L/mm
	287	27.5	50	10mm

Case 3	H/ μm	$t_1/\mu\text{m}$	$t_2/\mu\text{m}$	ϕ
	458	25	156	0.668
	H- $t_2/\mu\text{m}$	(G- $t_1)/\mu\text{m}$	G/ μm	L/mm
	320	28	50	10mm

Case study 2

In order to demonstrate the effectiveness of the above method, the constructal method was applied to model studies by Toh *et al.* [11] and Tuckerman and Pease [10]. The actual dimensions of the micro-channel heat sink and their volume fraction are shown in Table 3; the coolant was water and the conducting solid was silicon wafer with a thermal conductivity of 148 W/m K. The results obtained using the finite volume method is then compared with experimentally measured thermal resistance from different flow rates. The results of this work were then compared with the experimentally measured thermal resistance supplied by Tuckerman and Pease [10] using the local thermal resistance given in equation (10).

Table 3b reports the maximum thermal resistance for three cases tabulated in Table 3a. These thermal resistances were reported at $z = 9$ mm. Table 3b shows the comparison between the thermal resistance measured experimentally by Tuckerman and Pease [10] and numerically by Toh *et al.* [11], and those calculated [using equation (9)] in this study. The agreement with the experimental work is within 28% for case 1, 11% for cases 2 and 3, and with numerical results it is within 3%.

The micro-channel heat sink had three degrees of freedom, L, H/G, and t_1/t_2 . For the purposes of comparison, one degree of freedom was fixed, L, while the internal structure t_1/t_2 and the external shape were allowed to vary with the assumed pressure drop. The total volume of the unit micro-channel heat sink was fixed at $V = 0.215 \text{ mm}^3$, the axial length of the micro-channel was also fixed at 10 mm, and the unit cross-sectional area was 0.0215 mm^2 . The micro-channel heat sink was expected to occupy a total base surface area of $10 \text{ mm} \times 10 \text{ mm}$. The pressure drop (gage

pressure) across the unit cell was set at 117.2 kPa. The solid material was made of silicon substrate, and the fluid flowing through the channels was water. The thermal conductivity ratio is given as 246.7. Table 4 illustrates the reduction in thermal resistance obtained using the constructal design method. A reduction of 8% in thermal resistance was obtained by varying H/G and t_1/t_2 , while keeping L constant for the case given in Table 3.

Table 3b Comparison of thermal resistance at $x = 9\text{mm}$.

Cases	q'' (W/cm^2)	\dot{Q} (cm^3/s)	R ($\text{K}\cdot\text{cm}^2/\text{W}$)		
			Ref. [10]	Ref. [11]	Present Study
			Experiment	Simulation	
1	181	4.7	0.111	0.157	0.154
2	277	6.5	0.113	0.128	0.122
3	790	8.6	0.09	0.105	0.100

Table 4 Constructal method for a given micro-channel heat sink arrangement, for case 2 in Table 3

Pressure drop number ($\text{Be} = 2.9 \times 10^8$)	$\left(\frac{H}{G}\right)$				
	8.6	10	15	20	
$(t_1/t_2)_{\text{opt}}$	0.16	0.11	0.055	0.035	
R ($x = 1\text{cm}$, $\text{K}\cdot\text{cm}^2/\text{W}$)	0.122	0.117	0.113	0.121	
num = $\frac{W}{G}$	200	216	264	305	
Reduction in R (%)	-	4.3	7.6	0.22	
			OPTIMUM		

MULTISCALE PIN FINNS

Consider the two rows of a multi-scale cylindrical pin fin assembly as shown in Fig. 15. The distance between the first row of fins and the leading edge is S_1 . The distance between the two rows is S_2 . The fin heights are H_1 and H_2 , while their respective diameters are D_1 and D_2 . The swept length is L and it is fixed. The flow assembly is bathed by a free stream that is uniform and isothermal. Because of symmetry we select an elemental volume that contains only two fins on a rectangular wall base of swept length L and width $L/3$.

The objective is to discover the configuration (i. e. all the dimensions) such that the rate of heat transfer from the solid to the fluid is maximum subject to the constraint that the total volume of fin volume (V) is fixed

$$D_1^2 H_1 + D_2^2 H_2 = \frac{4}{\pi} V, \text{ constant} \quad (41)$$

This constraint is dictated by the weight and the material cost of the fins structure, which is a limiting parameter in the design of electronic devices and modern vehicles (e. g. aircraft, fuel efficient vehicles). In addition, there is the overall size constraint

$$S_1 + D_1 + S_2 + D_2 = L \quad (42)$$

The configuration has six dimensions that can vary (S_1, S_2, H_1, H_2, D_1 , and D_2). We fix S_1 such that the first fin is close to the leading edge, and this leaves five dimensions in the design. Because of the two constraints (1, 2), the number of degrees of freedom is three. The flow is assumed steady, laminar, incompressible and two-dimensional. All the thermo-physical properties are assumed constant. Equations (1-5) are non-dimensionalized by defining variables

$$(\tilde{x}, \tilde{y}, \tilde{z}) = \frac{(x, y, z)}{L} \quad (\tilde{u}, \tilde{v}, \tilde{w}) = \frac{(u, v, w)}{U_\infty} \quad (43)$$

$$\tilde{T} = \frac{T - T_\infty}{T_w - T_\infty} \quad \tilde{P} = \frac{P}{\mu U_\infty / L} \quad (44)$$

The dimension variable arising from the discretization are Pr , and Re [38], where Pr is the Prandtl number ν/α , and Re is the Reynolds number

$$Re = \frac{U_\infty L}{\nu} \quad (45)$$

The flow boundary conditions are: no slip and no penetration on the fins and the wall surfaces, and $\tilde{w} = 1$, $\partial\tilde{u}/\partial\tilde{z} = \partial\tilde{v}/\partial\tilde{z} = 0$ at the inlet of the flow assembly; $\partial(\tilde{u}, \tilde{v}, \tilde{w})/\partial\tilde{x} = 0$ at the exit and $\partial(\tilde{u}, \tilde{v}, \tilde{w})/\partial\tilde{y} = 0$, at the top of the computational domain and no flow and no penetration at the plane of symmetry. The thermal boundary conditions are: $\tilde{T} = 1$ on the wall surfaces, and $\tilde{T} = 0$ on the inlet plane of the computational domain. The planes of symmetry of the computational domain are adiabatic, that is $\left.\frac{\partial\tilde{T}}{\partial n}\right|_\Omega = 0$ on the plane of symmetry.

The spacing between the fins varies, and the shapes of the fins are allowed to morph. We are interested in the geometric configuration $(\tilde{D}_1, \tilde{D}_2, \tilde{H}_1, \tilde{H}_2, \tilde{S}_2)$ in which the overall heat transfer between the elemental \tilde{T}_w and the fin surfaces and the surrounding flow is a maximum. The dimensionless measure of the overall heat transfer is

$$\tilde{q} = \frac{q/L}{k(T_w - T_\infty)} \quad (46)$$

where q is the total heat transfer rate integrated over the surface of the fins and the elemental surfaces. This \tilde{q} formula is the dimensionless global thermal conductance of the volume element. Numerical procedure follows that described earlier in this paper see Refs. [36, 38].

Optimization of multi-scale pin fins

The search for optimal flow and heat sink configurations was organized in three nested optimization loops. The fin flow structure has three degrees of freedom which are designated as $\frac{H_2}{H_1}, \tilde{S}_2$ and $\frac{D_2}{D_1}$. We started by fixing the distance between the first fin and the leading edge, $\tilde{S}_1 = 0.05$, with the total volume of the fins set at $\tilde{V} = 0.01$. The degrees of freedom that remain are the ratios of the fins

height, $\frac{H_2}{H_1}$, and the diameters ratio $\frac{D_2}{D_1}$, and the spacing between the cylinders, \tilde{S}_2 . The dimensions of the flow structure are set as follows: the non-dimensionalized flow length \tilde{L} is set equal to 1, the flow width (the distance between two symmetry planes, in the x -direction) is $\tilde{L}/3$, and the virtual extension was fixed at $\tilde{H}_u = 0.2$.

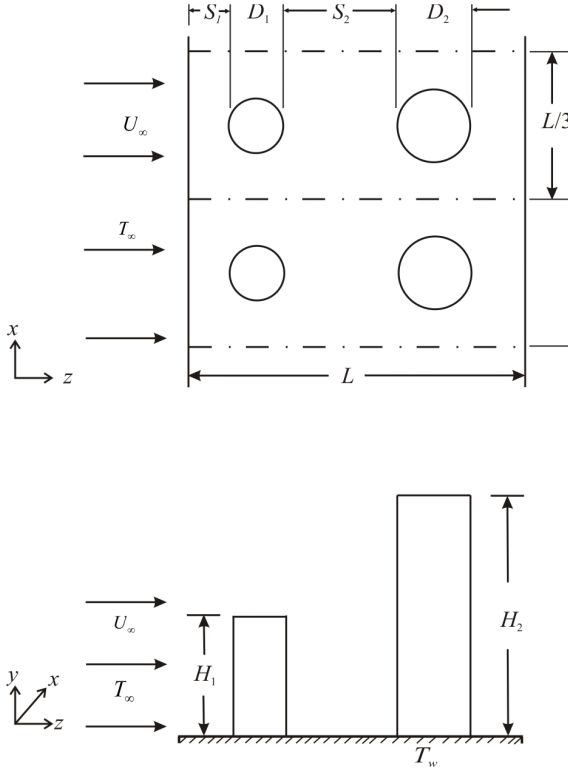


Figure 15 Two rows with unequal pin fins: Top: view from above; Bottom: view from the side

Figure 16 shows the influence of the Reynolds number on the optimal fin to fin distance $\tilde{S}_{2,opt}$ is insignificant over the Re range considered. Similarly, the optimal height ratio, $\left(\frac{H_2}{H_1}\right)_{opt}$ is robust, as the effect of Reynolds number on this parameter is fairly insignificant. In this range of Reynolds numbers $\left(\frac{H_2}{H_1}\right)_{opt}$ is equal to 0.9. It indicates that the height of the second row of fins should be slightly lower than that of the first rows. Figure 16 also shows that $\left(\frac{D_2}{D_1}\right)_{opt}$ increases with Re . This is an important result, as this establishes that the diameters of the fins must not be uniform. The results of Fig. 16 were correlated within an error of less than one percent by

$$\left(\frac{D_2}{D_1}\right)_{opt} = 0.62 Re^{0.146} \quad (47)$$

The maximum total heat transfer rate increases with the Reynolds number, and from Fig. 16 this trend was correlated with an error of less than one percent by

$$\tilde{q}_{max} = 2.16 Re^{0.32} \quad (48)$$

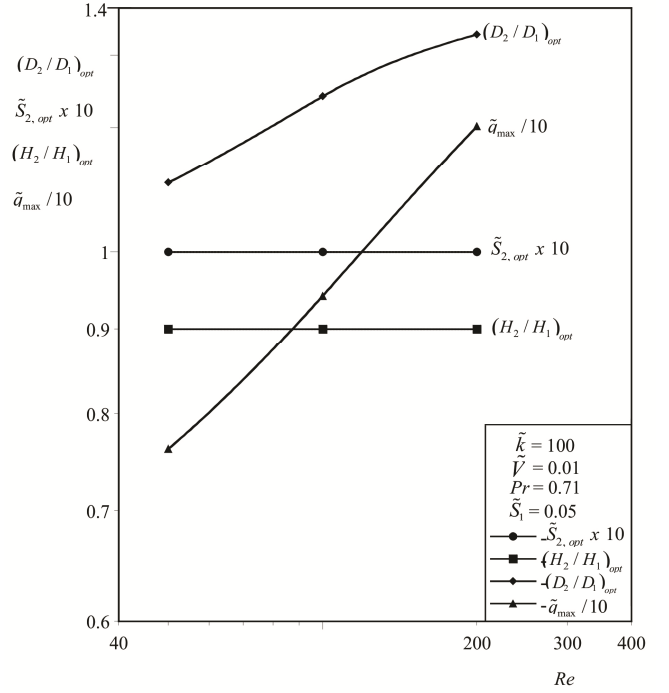


Figure 16 The optimal configurations and maximal total heat transfer rate for the rows of pin-fins in Figure 1.

Effect of dimensionless conductivity ratio

The effect of the thermal conductivity ratio \tilde{k} was also investigated. In Fig. 17 the results are reported for the range $30 \leq \tilde{k} \leq 300$ at a Reynolds number of 100. The figure shows that the optimal height ratio is fairly constant for the \tilde{k} range considered. The relationship between the dimensionless thermal conductivity and the optimal diameter ratio shows that as \tilde{k} increases the optimal diameter ratio decreases. This relationship is correlated by

$$\left(\frac{D_2}{D_1}\right)_{opt} = 2.54 \tilde{k}^{-0.16} \quad (49)$$

The optimal spacing between the pin fins shows that as \tilde{k} increases the optimal spacing $\tilde{S}_{2,opt}$ also increases. The effect of \tilde{k} on the maximum total heat transfer rate shows a similar trend as with respect to the Reynolds number. From Fig. 17 this can be correlated with an error of less than one percent by the relation

$$\tilde{q}_{max} = 2.48 \tilde{k}^{0.29} \quad (50)$$

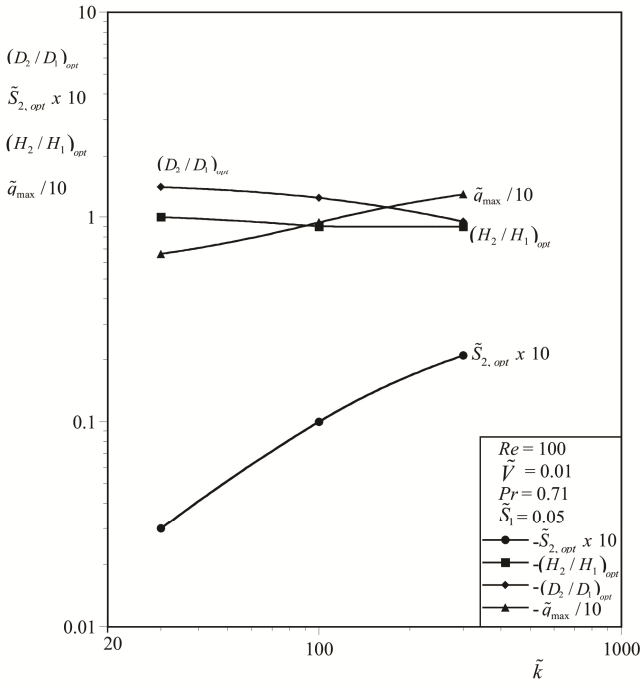


Figure 17 The optimal configurations and maximal total heat transfer rate for the rows of pin-fins in Figure 1.

The scaling trends discovered numerically in the preceding sections can be explained on the basis of scale analysis [38]. The scaling from [38], shows that

$$\frac{D_1}{D_2} \sim \left(\frac{H_1}{H_2} \right)^2 \quad (51)$$

and, the ratio of diameters should be

$$\frac{D_1}{D_2} \sim \frac{\Delta T_1}{\Delta T_2} \geq 1 \quad (52)$$

This conclusion agrees in an order of magnitude sense with the data plotted in Figs. 16 and 17. The ratio $\frac{D_1}{D_2}$ becomes

smaller than 1 when \tilde{k} increases (Fig 17) and when Re decreases

Case Study For Micro-Pin fins

Figure 18 gives the physical model of double row micropin-fin geometry. The two fins of varying diameters D_1 and D_2 and respective heights H_1 and H_2 spaced at a distance s from each other aim to enhance the extraction of heat supplied to the base of the thermal conductive material at a temperature T_w . Air, which is uniform and isothermal, is driven across the heat sink of fixed flow length L and width

Figure 19 shows vertically arranged pin-fins form part of a three-row-finned array with row-specific diameters D_1 , D_2 and D_3 respectively. The various rows are spaced by a distance s_1 and s_2 as depicted in Figure 12. Uniform row height assumption was made (from results obtained from case one and scale analysis). Therefore, $H_1 = H_2 = H_3$. The detailed report on this geometry are presented in Ref. [36]. The mass, momentum and energy conservation equations were solved over the discretised domain shown in Figures 16 and 17. Using a combination of CFD, Matlab and Dynamic Q optimize. The double and triple rows micro pin

fins were optimized. For the sake of brevity we shall only report on the heat transfer rate from both structures.

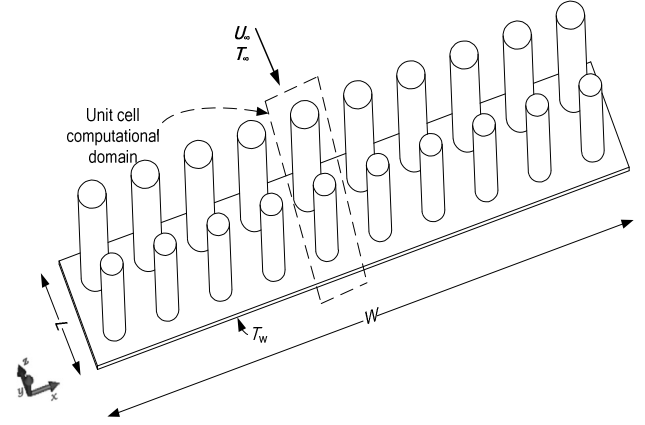


Figure 18 Physical model of a double row finned heat sink

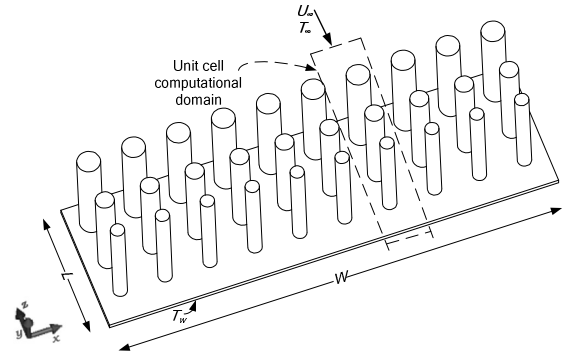


Figure 19 Physical model of a triple variable row micropin-fin heat sink

Figures 20a and 20b shows the effect of Reynolds number and conductivity ratio on the heat transfer for both the optimized double row fins and triple row micro pins, it is observed that as the Reynolds number increases the heat transfer rate also increases. The triple rows pin fins have a larger heat transfer rate when compared to the double rows micro pin fins. The same behaviour is observed for figure 20b, that the triples row micro pin fins gives a higher heat transfer as the thermal conductivity ratio increases.

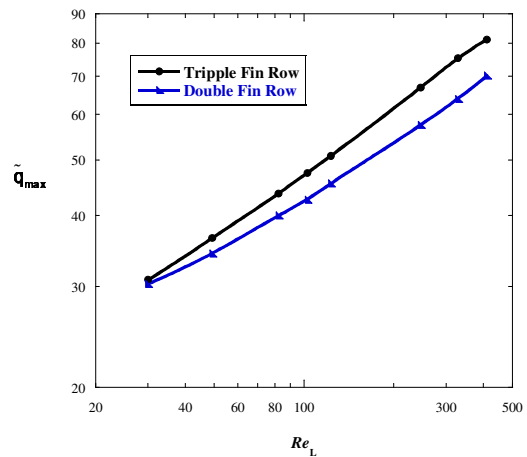


Figure 20a

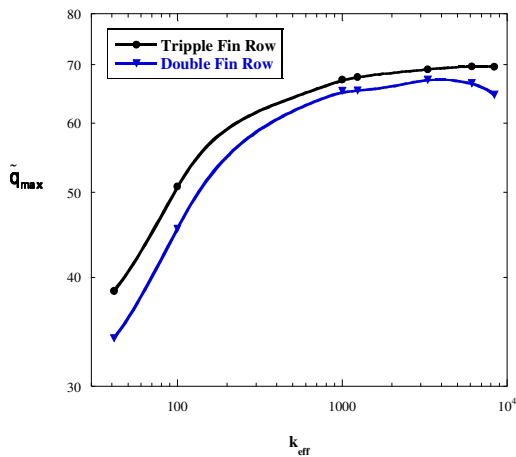


Figure 20b A summarised look at the thermal performance of a micropin-fin heat sinks

CONCLUSIONS

In this paper, we showed numerically and theoretically that the global thermal conductance for two types of micro-channel heat sinks can be maximised by optimising the aspect ratio, H/G , the axial length, \tilde{L}_{opt} and therefore the channel hydraulic diameter for laminar forced conjugate heat transfer. The micro-channel heat sinks are conjugate problems with conduction in the solid and forced convective flow in the cooling liquid. We started the constructal design of the heat sink cooling channel from an elemental unit cell, and optimised the internal and external structure of the unit cell. This optimal configuration can be further arranged or assembled in a stack to form a larger construct, depending on the required total volume.

Numerical optimisation results further show that the optimal micro-channel shape ($D_{h,opt}$), minimised peak temperature (maximised global thermal conductance), aspect ratio and the axial length are functions of the applied pressure difference and solid volume fraction.

Comparisons of the results obtained numerically with approximate solutions based on scale analysis with those work obtained from literature show excellent agreement for optimal micro-channel dimensions.

In the third part of this paper we described the procedure for the conceptual design of a new generation of multi-scale pin arranged in a row using the principles of constructal theory. The pin-fins are cooled by laminar forced convection. The total fin volume of the pins was fixed. Numerical optimization was performed to determine the optimal configuration (relative diameters, heights and spacings between fins). The optimized configuration is the result of balancing conduction along the fins with convection transversal to the fins. The resulting flow structure has multiple scales that are distributed non-uniformly throughout the flow structure.

The results predicted by using scale analysis are in agreement with the numerical results. In conclusion, the pin-fins flow structure performs best when the pin-fin diameters and heights are non-uniform.

In summary it is expected that the conceptual design of micro-channel heat sinks and micro pin fins using the constructal method will lead to better and faster design of

micro-channel heat sinks with improved performance and higher global thermal conductance (minimised global resistance) and heat transfer rate.

Acknowledgements

Prof. Bello-Ochende acknowledges the support received from the University of Pretoria and the National Research Foundation of the Republic of South Africa.

Reference:

- [1] Dirker, J., Liu W., Van Wyk D., Meyer J. P. and Malan A. G., modules, *IEEE Transaction on Power Electronics Embedded solid state heat extraction in integrated power electronic*, Vol. 3 20, 2005, pp. 694 – 703.
- [2] Webb, R., Next generation devices for electronic cooling with heat rejection to the air, *Journal of Heat Transfer*, v 127, 2005, pp. 2 - 9.
- [3] Hetsroni, G., Mosyak, A., Pogrebnyak, E. and Yarin, L. P., Heat transfer in micro-channels: Comparison of experiments with theory and numerical results, *International Journal of Heat Mass Transfer*, vol. 48, 2005, pp. 5580-5601.
- [4] Bejan, A., *Shape and Structure, from Engineering to Nature*, Cambridge University Press, Cambridge, UK, 2000.
- [5] Bejan, A. and Lorente, S., Constructal theory of generation and configuration in nature and engineering, *Journal of Applied Physics*, Vol. 100, 2006, pp. 041301.
- [6] Bar-Cohen, A. and Rohsenow, W. M., Thermally optimum spacing of vertical, natural convection cooled, parallel plates, *ASME Journal of Heat Transfer*, Vol. 106, 1984, pp. 116-123.
- [7] Bejan, A., *Convection Heat Transfer*, 3rd edn, Wiley, New York, 2004.
- [8] Bello-Ochende, T. and Bejan, A., Fitting the duct to the “body” of the convective flow, *International Journal of Heat and Mass Transfer*, Vol. 46, 2006, pp. 1693-1701.
- [9] Bejan, A. and Sciubba, E., The optimal spacing for parallel plates cooled by forced convection, *International Journal of Heat Mass Transfer*, Vol. 35, 1992, pp. 3259-3264.
- [10] Tuckerman, D. B. and Pease, R.F.W., High-performance heat sinking for VLSI, *IEEE Electron, Dev. Lett. EDL-2*, 1982, pp. 126 – 129.
- [11] Toh, K. C., Cheng, X. Y. and Chai, J. C., Numerical computation of fluid flow and heat transfer in microchannels, *International Journal of Heat Mass Transfer*, Vol. 45, 2002, pp. 5133-5141.
- [12] Qu, W. and Mudawar, I., Analysis of three-dimensional heat transfer in micro-channel heat sinks, *International Journal of Heat Mass Transfer*, Vol. 45, 2002, pp. 3973-3985.
- [13] Knight, R. W., Hall, D. J., Goodling, J. S. and Jaeger C. J., Heat sink optimization with application to microchannels, *IEEE Transaction of Component, Hybrids, and Manufacturing Technology*, Vol. 15 (5) 1992, pp. 832 – 842.
- [14] Fedorov, A. G. and Viskanta, R., Three-dimensional conjugate heat transfer in the micro-channel heat sink for electronic packaging, *International Journal of Heat Mass Transfer*, 2000, pp. 43, 399-415.

- [15] Li, J., Peterson, G. P. and Cheng, P., Three-dimensional analysis of heat transfer in a micro-heat sink with single phase flow, *International Journal of Heat Mass Transfer*, Vol. 47, 2004, pp. 4215 – 4231.
- [16] Tou, S. K. W., Tso, C. P. and Zhang, X., 3-D numerical analysis of natural convective cooling of a 3×3 heater array in rectangular enclosures, *Int. J. Heat Mass Transfer*, Vol. 44, 1999, pp. 3231 – 3244.
- [17] Kawano, K., Minikami, K., Iwasaki, H. and Ishizuka, M., Micro channel heat exchanger for cooling electrical equipment, Application of Heat Transfer in Equipment, Systems and Education, *ASME HTD*, Vol. 361-3/PID-3, 1998, pp.173-180.
- [18] Foli, K., Okabe, T., Olhofer, M., Jin, Y. and Sendhoff, B., Optimization of micro heat exchanger: CFD, analytical approach and multi-objective evolutionary algorithms, *International Journal of and Heat Mass Transfer*, Vol. 49, pp. 1090-1099.
- [19] Favre-Marinet, M., Le Person, S. and Bejan, A., Maximum heat transfer rate density in two-dimensional mini-channels and micro-channels, *Microscale Thermophysical Engineering*, 2004, pp. 225-237.
- [20] Bhattacharjee, S. and Grosshandler, W. L., The formation of wall jet near a high temperature wall under microgravity environment, *ASME HTD*, Vol. 96, 1988, pp. 711-716.
- [21] Petrescu, S., Comments on the optimal spacing of parallel plates cooled by forced convection, *International Journal of Heat Mass Transfer*, Vol. 37 1994, pp. 1283.
- [22] Patankar, S. V., Numerical Heat Transfer and Fluid flow, Hemisphere, New York, 1980.
- [23] Muzychka, Y. S., Constructal design of forced convection cooled micro-channel heat sinks and exchanger, *International Journal of Heat Mass Transfer*, Vol. 48, 2005, pp. 3119 – 3124.
- [24] T. Bello-Ochende, L. Liebenberg, A. G. Malan, A. Bejan, J. P. Meyer, Optimal geometry for conjugate heat transfer in a cooling channel, proceeding of the 13th International Heat Transfer Conference, 13-18 August, Sydney 2006.
- [25] T. Bello-Ochende, J. P. Meyer, Combined micro-channel heat sink optimization for cooled electronics, proceeding of *ASME-HTD conference*, July 8-12, Vancouver, Canada, Vol. 2, 2007, pp. 661 -669
- [26] Bello-Ochende, T., Liebenberg, L., and Meyer, J. P., 2007, Constructal cooling Channels for micro-channel heat sinks, *International Journal of Heat and Mass Transfer*, Vol. 50, pp. 4141–4150.
- [27] Shah, R. K. and London, A. L., Laminar Flow Forced Convection in Ducts, Academic Press, NY, 1978, pp. 78-283.
- [28] Yilmaz, A., Buyukalaca, O. and Yilmaz, T., Optimum shape and dimensions of channel for convective heat transfer in laminar flow at constant wall temperature, *International Journal of Heat Mass Transfer*, Vol. 43, 2000, pp. 767 – 775.
- [29] Bejan, A., Advanced Engineering Thermodynamics, 3rd edition, Wiley, New York, 2007.
- [30] Bejan, A. and Almogbel, M., Constructal T-shape fins, *Int. J. Heat Mass Transfer*, 2000, 43, 2101 – 2115.
- [31] Culham, J. R. and Muzychka, Y. S., Optimization of plate fin heat sinks using entropy generation and minimization, *IEEE transaction CPT*, Vol. 24(2), 2001, pp. 159 – 165.
- [32] T. Bello-Ochende, L. Liebenberg, A. G. Malan, A. Bejan, J. P. Meyer, Optimization of conjugate heat transfer in three dimensional cooling channels, *Journal of Enhanced Heat Transfer*, Vol. 14(4), 2007, pp. 279-293.
- [33] Bello-Ochende, T. and Bejan, A., Optimal spacing for mixed convection, *ASME Journal of Heat Transfer*, Vol. 126, 2004, pp. 957-962.
- [34] T. Bello-Ochende, J.P. Meyer, F.U. Ighalo, Combined Numerical Optimization and Constructal Theory for the Design of Microchannel Heat Sinks, *Numerical Heat Transfer*, Part A, Vol. 58, 2010, pp. 882–899.
- [35] Ordonez, J. C., Integrative Energy-System Design: System Structure from Thermodynamic Optimization. Ph. D. Thesis, Duke University, Durham, NC, ch. 6, 2003.
- [36] Ighalo, F. U. Optimisation of Microchannels and Micropin-fin Heat Sinks with Computational Fluid Dynamics in Combination with a Mathematical Optimisation Algorithm, Master Thesis, 2011.
- [37] Bello-Ochende, T and Meyer, J. P., Constructal cooling channels: application to heat transfer in micro-channel heat sinks, *International Journal of Emerging Multidisciplinary Fluid sciences*, Vol. 1 (1), 2009, pp. 61-83.
- [38] Bello-Ochende, T. Meyer, J. P., Bejan, A., *Constructal multi-scale pin fins*, *International Journal of Heat and Mass Transfer*, Vol. 53, 2010, pp. 2773–2779.